Sustainable Chemistry and Pharmacy 29 (2022) 100746

Contents lists available at ScienceDirect

Sustainable Chemistry and Pharmacy

journal homepage: www.elsevier.com/locate/scp

Comparative study of alkali activated cements based on metallurgical slags, in terms of technological properties developed

M.A. Gómez-Casero [a,c,*], L. Pérez-Villarejo [b,c], P.J. Sánchez-Soto [d], D. Eliche-Quesada [a,c]

[a] Department of Chemical, Environmental, and Materials Engineering, Higher Polytechnic School of Jaén, University of Jaén, Campus Las Lagunillas s/n, 23071, Jaén, Spain
[b] Department of Chemical, Environmental, and Materials Engineering, Higher Polytechnic School of Linares, University of Jaen, Campus Científico-Tecnológico, Cinturón Sur s/n, 23700, Linares, Spain
[c] Center for Advanced Studies in Earth Sciences, Energy and Environment (CEACTEMA), University of Jaén, Campus Las Lagunillas, s/n, 23071, Jaén, Spain
[d] Institute of Materials Science of Sevilla (ICMS), Joint Center of the Spanish National Research Council (CSIC)-University of Sevilla, 41092, Sevilla, Spain

ARTICLE INFO

Keywords:
Alkali activated cements
Steel slag
Copper slags
Circular economy

ABSTRACT

In this work, an investigation on the use of two slags from different origins (electric arc furnace slag (EAFS) and copper slag (CS)) as raw materials in the manufacture of alkali-activated cements has been carried out. A comparison of the different mechanical properties developed by the alkaline activation of each raw material has been studied. Combination of 35 wt% potassium hydroxide (KOH) solution with different concentration (5, 8, 12 and 15 M) and 65 wt% potassium silicate (K_2SiO_3) solution was used as activating solution to manufacture alkali activated cements. The pastes were cured 24 h in a climatic chamber at 20 °C at 90% of relative humidity, subsequently demoulded and cured at same condition during 1, 7, 28 and 90 days. Alkali activated materials have been characterized using Fourier transform infrared spectroscopy (FTIR), X-ray diffraction (XRD) and scanning electron microscopy (SEM). The physical properties: bulk density, water absorption and apparent porosity, mechanical properties, flexural strength and compressive strength and thermal properties: thermal conductivity have been determined. The results indicate that two types of slags studied are a suitable source of aluminosilicates that can be activated for the manufacture of alkali-activated materials. These precursors are capable of developing high values of flexural and compressive strength and low values of thermal conductivity when optimal concentration of KOH was used. The optimal composition was developed when CS was utilized. Binders with CS and 12 M M ratio achieved compressive strength values up to 70 MPa.

1. Introduction

Cement is one of the most used materials in civil engineering, where the most used is Portland cement (PC). This cement has high strength properties and durability (Puertas et al., 2018). However, its manufacture has a high environmental cost, because it need high temperatures to produce it and extraction in quarries of the raw material (Szab ó et al., 2006). This implied a high emission of CO_2 to

* Corresponding author. Department of Chemical, Environmental, and Materials Engineering, Higher Polytechnic School of Jaén, University of Jaén, Campus Las Lagunillas s/n, 23071, Jaén, Spain.
E-mail address: magomez@ujaen.es (M.A. Gómez-Casero).

https://doi.org/10.1016/j.scp.2022.100746
Received 14 January 2022; Received in revised form 31 May 2022; Accepted 9 June 2022
Available online 23 June 2022

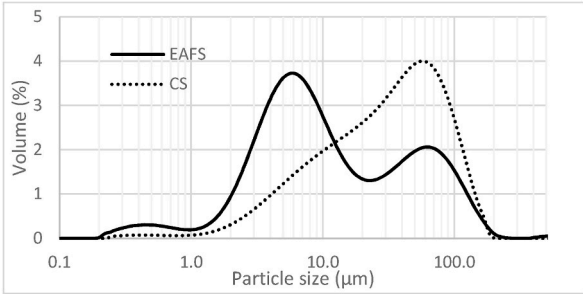

Fig. 1. Particle size distribution of raw materials.

the atmosphere, the main greenhouse gas, but also NOx. The search for alternatives to Portland cement has led to many studies on new materials for construction. The target is to produce new materials more environmentally friendly.

In recent years, many studies have emerged to reduce CO_2 emissions and replace PC with more environmentally friendly binders (Hajimohammadi et al., 2017; Amari et al., 2019). An alternative are geopolymers (Provis, 2018) or alkali activated cements (AAC), they are consider the new green cementitious materials (Li et al., 2021). AAC are manufactured as a combination of alumina-silicate source (precursor) and alkaline activator solution (Fakhrabadi et al., 2021). Aluminosilicates are dissolved in highly alkaline environments forming an amorphous semi-crystalline 3D silicoaluminate polymeric structure (Sithole and Mashifana, 2020a). Alkali-activated cements are manufactured as a combination of calcium-silicate source (precursor) and alkaline activator solution being the main reagent product calcium silicate gel (C–S–H). These cements have given good results in relation to their strength and durability (Pacheco-Torgal et al., 2012), but their behaviour is different depending on the material used and its provenance.

Several materials have been used as precursor in geopolymers and alkaline activated materials. Any examples are industrial waste, by-product, ashes, slags and natural sources as clays (Rees, 2007; Aredes et al., 2015; Nikolov et al., 2017; Seo et al., 2020). The target using these materials is to delete waste produced in the industry and reduce CO_2 emissions. The use of slag has been extensively studied in previous works (Mozgawa and Deja, 2009; Asim et al., 2019; Sithole and Mashifana, 2020b; Ameri et al., 2021). Slag has different origin according to metallurgical process used: ground granulated blast furnace slag (GGBFS), electric arc furnace slag (EAFS) or black steel slag, secondary metallurgical slag such as ladle furnace basic slag (LS), also called white slag, basic oxygen furnace slag (BOS) and other slags (Lancellotti et al., 2021).

Historically, one of the most used slags as aluminosilicate and calcium precursor are GGBFS so, these slags have been used alone and mixed with class F fly ash (Luukkonen et al., 2018). Nevertheless, other slags have been used as stainless steel slag with different results depending of activator and curing condition performed (Salman et al., 2014, 2015). Steel production is one of the most important economic activities for industrial development; however, it represents great challenges related to the impact generated on the environment as millions of tons of slag are generated worldwide. EAFS is a by-product of steel production, during steel making process, when molten steel and impurities are separated (Khan et al., 2016). The main chemical components of EAFS are CaO, SiO_2 and Fe_2O_3 and a small amount of Al_2O_3 (Wang et al., 2021; Oyebisi et al., 2020). EAFS have been used to produce binder mixed with other materials (Abdel-Ghani et al., 2018; Furlani et al., 2018; Guo and Yang, 2020). Also they have been mixed with carbon ashes or replacing Portland cement to manufacture mortar or concrete (Wang et al., 2021; Martins et al., 2021).

Cooper slag is generated during the refining process of copper (Singh and Singh, 2020a). CS is rich in FeO, Fe_2O_3 and SiO_2, but also it contains various other elements such as Al, Ca, Mg and Cu in metallic or oxide/sulphide forms (You et al., 2020; Yan et al., 2021). Although the chemical composition vary from plant to plant and mineral additions may be limited by their local availability (Salman et al., 2015). On the other hand, regarding the another wastes used is this work, copper slag, there are in recent years, several works about its use as precursor for alkali cementitious material (Singh and Singh, 2019), in the manufacture of mortars and for producing alkaline activated cements (Singh and Singh, 2020b; Nazer et al., 2016; Khan et al., 2021).

Chemical activators most used in AAC are sodium and potassium hydroxide. Adding sodium or potassium silicate (respectively) to these solutions, better results in terms of mechanical strength are obtained (Puertas, 1995). The proportion of activator depends on raw materials used (Nedunuri and Muhammad, 2021) and it necessary a previous study.

In this work, a comparative study is performed between these two slags with different sources, electric arc furnace slags (EAFS) and copper slags (CS). Alkali activated pastes were cured in room temperature. As activator, a solution mixing K_2SiO_4 and KOH with four different concentration were used. The reactivity, thus a comparison of the different physical, mechanical and thermal properties developed by alkali activated cements has been studied.

2. Materials and methods

2.1. Raw materials and characterization

The electric arc furnace slags (EAFS) comes from Siderúrgica Sevillana S.A. industry, located in San Juan de Aznalfarache (Seville, Spain). This industry valorises ferrous scrap to convert it into steel bars of different profiles, diameters and qualities. This material is produced in electric arc furnace during the melting process of ferrous scrap and it has a grain size of 4–5 mm.

The copper slags (CS) was supplied by Atlantic Copper Smelting and Refinery, situated at Huelva (Spain). This industry

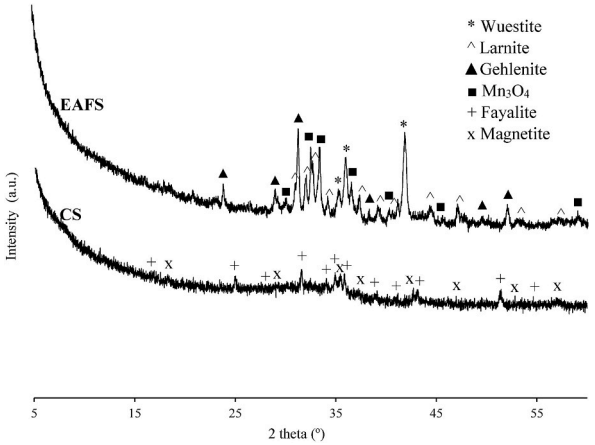

Fig. 2. XRD spectrum of precursors: EAFS and CS.

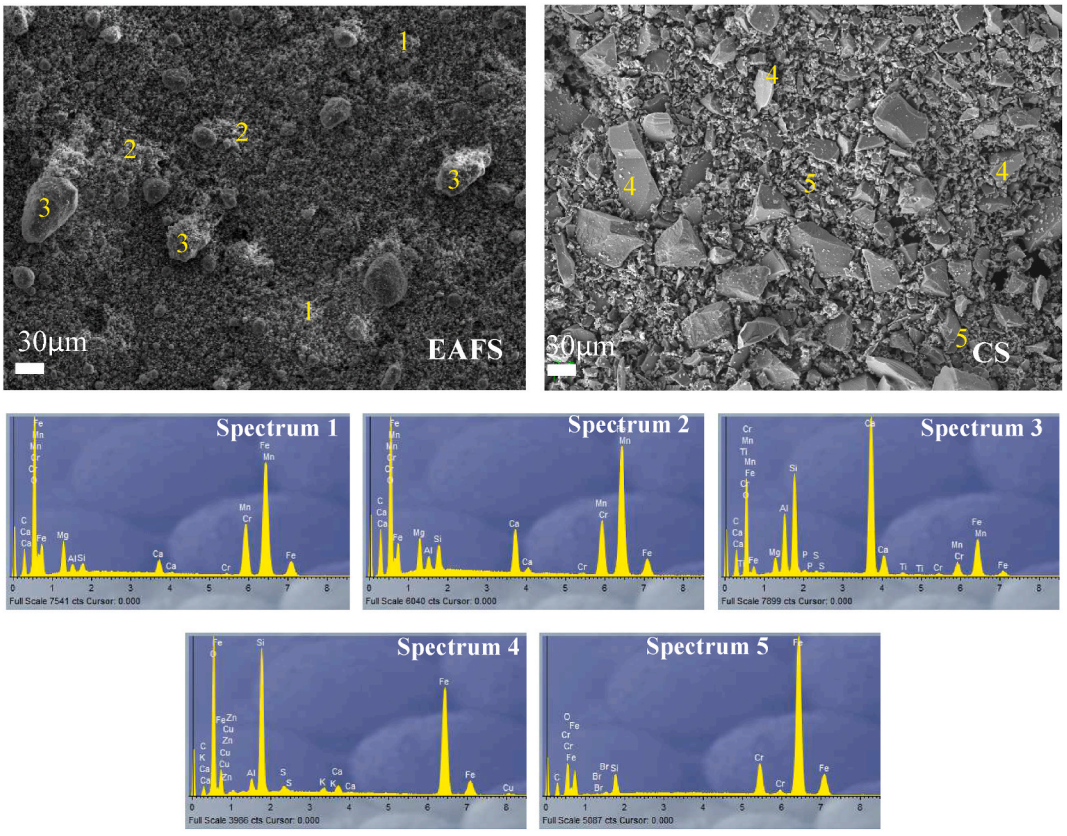

Fig. 3. SEM images of precursors.

manufacture refined copper and they obtain other products as sulphuric acid, precious metals and iron silicate (copper slags). These slags were provided with a maximum particle size of 4 mm.

Due to grain size, both slags had to be crushed, after that, the resulting materials were put in a ball mill. Subsequently were sieved below 100 μm. Laser diffraction analysis was used to obtain the particle size distribution of slags (Fig. 1). For this purpose, a Malvern Mastersizer 2000 laser diffractometer was used. CS particles have more homogeneous distribution and a higher mean particle size (D_{50} = 30.5 μm) than EAFS particles with a slightly lower mean particle size (D_{50} = 8.7 μm) and more heterogeneous particle size distribution.

Crystalline mineralogical phases of raw materials was identified by Empyrean equipment with a PIXcel-3D detector from PANalytical using Cu K radiation (λ = 1.5406 Å) at a voltage of 40 kV and an amperage of 40 mA, a 2 theta range of 10–60° and a step size of

Table 1
Chemical composition (wt%) of precursors.

Precursor (wt %)	SiO_2	Al_2O_3	Fe_2O_3	CaO	MgO	MnO	Na_2O	K_2O	TiO_2	P_2O_5	SO_3	LOI
EAFS	17.29	10.71	24.16	30.89	2.63	5.68	0.16	0.03	0.79	0.41	0.28	5.39
CS	27.65	2.04	62.18	1.25	0.38	0.03	0.63	0.56	0.21	0.04	0.90	0.00

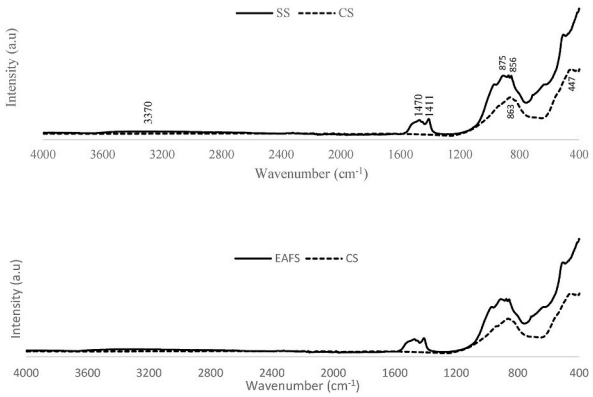

Fig. 4. FTIR spectra of raw materials: a) Electric Arc Furnace Slag, and b) Copper Slag.

0.02. The phase identification was performed using HighScore software. EAFS and CS present an amorphous structure as indicated by the deviation from the baseline, structure obtain in other studies (Lang et al., 2021). EAFS present as crystalline mineralogical phases wuestite (FeO), larnite (Ca_2SiO_4) and gehlenite ($Ca_2Al(SiAl)O_7$), it is consistent with other studies (Nikoli ć et al., 2020; Elkhachine et al., 2022). Although traces of manganese oxide (Mn_3O_4) were also detected, this presence is according with Balaguera et al. (Balaguera and Botero, 2020). In CS were identified diffraction peaks of fayalite ($(Fe^{2+})_2SiO_4$) and magnetite (Fe_3O_4) (Fig. 2). This agrees with the main minerals found by other authors in copper slags (Fakhrabadi et al., 2021; Singh and Singh, 2019; Phiri et al., 2021; Zheng et al., 2021).

The micrographs of the raw materials were obtained by Scanning Electron Microscopy (SEM) using a JEAL model SM 840 assisted by Energy Dispersive X-ray spectroscopy (EDS). The precursors were placed on an aluminium grid and the JEOL JFC 1100 sputter coater was used to coat with carbon. Spherical and irregular particles can be observed in the EAFS waste. Angular particles can be observed in CS waste. In both precursors, particles of different sizes can be observed. Smaller particle sizes were observed in the EAFS waste according to the particle size distribution data obtained (Fig. 3). Besides, the microanalysis performed on the selected samples showed at Fig. 3, revealed the presence of iron-rich particles (spectrums 1 and 2) and particles rich in calcium, silica and aluminium (spectrum 3) in EAFS micrograph, which is accordingly with XRF carried out (Table 1), as well as fayalite and magnetite in CS (spectrums 4 and 5), according to XRD analysis.

Results present in Table 1 correspond to chemical composition of precursors. Data were obtained by X-Ray fluorescence (XRF) using a Philips Magix Pro model PW-2440. Predominant components of EAFS are CaO (30.89 wt %) and Fe_2O_3 (24.16 wt %), with a high percentage of SiO_2 (17.29 wt %) and Al_2O_3 (10.71 wt %). Other oxides are also present in small amounts such as MgO (2.63 wt %) and MnO (5.68 wt %). In the case of CS slag, predominant oxides are Fe_2O_3 (62.18 wt %), followed by SiO_2 (27.65 wt %). Also small amounts of Al_2O_3 (2.04 wt %) and CaO (1.25 wt %) are present.

ATR-FTIR was performed using a Vertex 70 Bruker in the range 400–4000 cm^{-1}. FTIR spectra for raw materials are presented in Fig. 4. In EAFS a band centred at 3370 cm^{-1} was found and it can attribute to O–H bonds (Zhang et al., 2022). Silicate phases are confirmed with the presence of Si–O–Si bonds found by band at 1470 cm^{-1} and 975 cm^{-1} (Lang et al., 2021). Carbonate ion CO_3^{2-} were observed at 1411 cm^{-1} (Nikoli ć et al., 2020). The band centred at 856 cm^{-1} is attributed to bending vibration of SiO_4^{4-}, corresponding to larnite (Balaguera and Botero, 2020). At 875 cm^{-1} is find a band that it indicate the presence of Fe–O bonds (Balaguera and Botero, 2020). To CS bands at 863 and 447 cm^{-1} were found, they are attributed to stretching peak of Fe–Si–O (Zhang et al., 2021). Also the band 863 cm^{-1} can be attribute to SiO_4 tetrahedron in fayalite (Yan et al., 2021). This is consistent with results of XRD and it is according to results shown by Nazer et al. (2016).

2.2. Manufacture of alkali activated cements

The reactivity of slags and mechanical properties were compared, using different activating solutions. Alkaline activator used were a solution of 35 wt% potassium hydroxide with different concentration (5 M, 8 M, 12 M and 15 M) and 65 wt% potassium silicate. The potassium hydroxide with 85% of purity was supplied by GlobalChem company, and potassium silicate solution was supplied by Roth company with a composition of 7.5–8.7 wt % K_2O, 19.5–21.8 wt % SiO_2 and 69.5–73.0 wt % H_2O and a density of 1250 kg/m^3. The silica modulus obtained, pH measured and liquid/binder ratio used are presented in Table 2. The pH was determined with a Crison Basic 20 pH-meter. Different liquid/binder (l/b) ratios were used in order to obtain adequate workability. Alkali activated cements

Table 2
Design of alkali activated cements.

Alkali activated cements	Precursor used	Molarity of KOH	Raw material (g)	KOH (g)	H_2O (g)	K_2SiO_3 (g)	Ms	l/b ratio	CaO/FeO	$\frac{(Feo + Cao)}{Sio_2}$
EAFS-5M	EAFS	5 M	400	20.84	63.16	156	1.70	0.60	16.34	1.39
EAFS-8M		8 M		29.03	54.97	156	1.38			
EAFS-12M		12 M		37.13	46.88	156	1.17			
EAFS-15M		15 M		41.79	42.21	156	1.08			
CS-5M	CS	5 M	500	15.20	46.05	113.75	1.70	0.35	0.06	0.76
CS-8M		8 M		21.16	40.09	113.75	1.38			
CS-12M		12 M		27.07	34.18	113.75	1.17			
CS-15M		15 M		30.47	30.78	113.75	1.08			

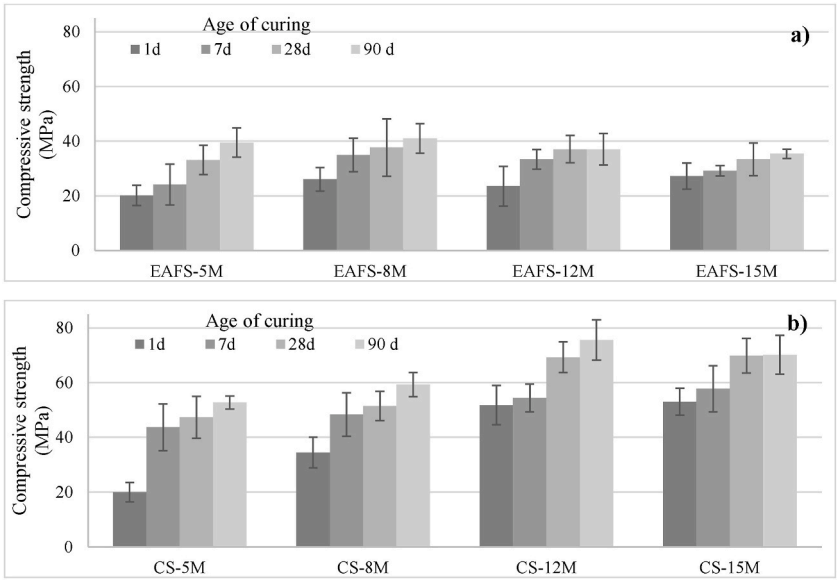

Fig. 5. Compressive strength over time for EAFS (a) and CS (b) alkali activated cement.

were named by EAFS or CS depending on the precursor used followed by the molarity of the KOH solution used. For example EAFS-5M is the alkaline cement manufactured using EAFS as raw material and employing an activating solution 65 wt% K_2SiO_3 and 35 wt% KOH with a 5 M concentration.

A Proeti planetary mixer was used to mix raw materials and alkaline activator solution for all compositions. The sequence was as follow: dry raw materials and activator solution were mixed at low speed for 90 s. Subsequently, the walls of the container were stirred and the mixture was mixed again for 30 s at low speed. The paste manufacture was sloped into 60x10x10 mm stainless steel moulds to determine physical and mechanical properties and cylindrical moulds with 55 mm in diameter and 15 mm in height to determine thermal conductivity, and then subjected to 60 strokes on a Proeti beating table to eliminate bubbles and achieve better compaction of the material.

A climatic chamber Daihan ThermoStable STH-305 was used for ageing the moulded pastes for 24 h. The climatic conditions imposed in the chamber were 90% relative humidity and 20 ± 1 °C. Subsequently, the hardened pastes were demoulded and cured in the climatic chamber at same conditions. Samples were maintained until the curing age 7, 28 and 90 days.

2.3. Experimental methods

The specimens were subjected to flexural strength tests following the standard UNE-EN 1015–11:2000/A1:2007 (UNE-EN 1015, 2007). A MTS Insight 5 machine (5 kN capacity) with a displacement speed of 0.2 mm/min was used. In total, four samples of each composition and curing time were tested. After flexural strength test, one-half was selected to obtain the mechanical compressive strength, and the other half to determine the bulk density. The compressive strength was carried out on the universal testing machine MTS 8101 (100 kN), according to the UNE-EN 1015–11:2000/A1:2007 standard (UNE-EN 1015, 2007).

The standard UNE-EN 1015–10 (UNE-EN 1015-10:1999, 1999) was used to determine the bulk density, apparent porosity and absorption of specimens according to the Archimedes principle. The average of four determinations of each half sample was calculated. The thermal conductivity of 55 mm diameter and 15 mm height specimens after 28 days of curing was determined using a FOX 50 TA instruments heat flow meter, according to ISO 8302 (ISO 8302).

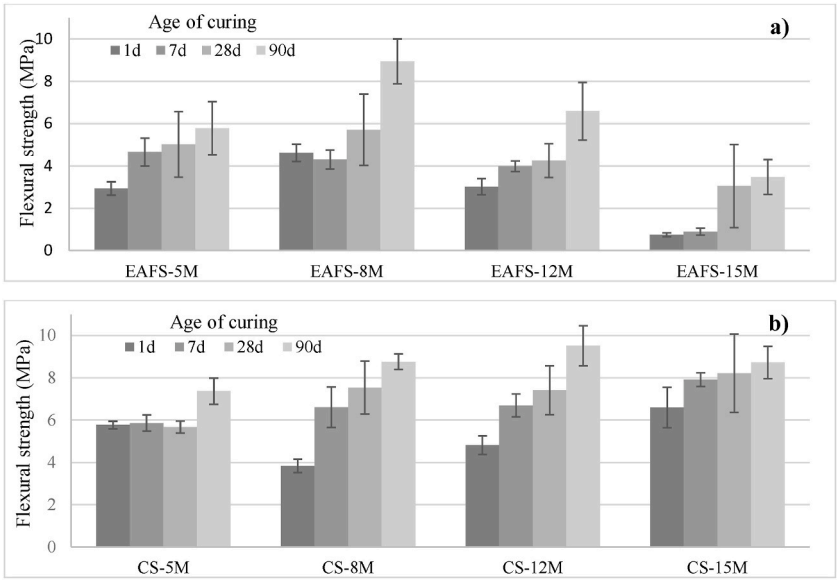

Fig. 6. Flexural strength over time for EAFS (a) and CS (b) alkali activated cement.

The reactivity of slags was determined according to the procedure followed by Bonet-Martínez et al. (Bonet-Mart í nez et al., 2020). To determine the degree of reaction of the hardened specimens, 1 g of ground and sieved sample (100 μm) was attacked with a HCl solution (1:20). The geopolymeric gel formed is dissolved in the solution, which is then filtered, dried and calcined at 1000 °C (3 h). The reaction degree is obtained from the equation (1):

$$\text{Degree reaction}(\%) = \text{1-calcined mass}*100 \quad (1)$$

The carbonate content has been determined by Bernard calcimeter was used. Results shown that EAFS has a high carbonate content (27.5%), while CS has a less value (7.9%). Also XRD, Attenuated Total Reflectance Fourier Transform Infrared Spectroscopy (ATR-FTIR) and SEM-EDS was used to determine hydration products. Powder samples (≤100 μm) were used in XRD and ATR-FTIR analysis. XRD ATR-FITR analysis were applied using the same equipment and operating conditions as for the raw materials.

3. Results and discussion

3.1. Mechanical strength: compressive and flexural strength

The main property in building materials are mechanical strength: compressive and flexural strength. The evolution of compressive strength as a function of curing age and molar concentration of KOH is presented in Fig. 5. Differences can be observed depending on the precursor used. When CS waste is used as a precursor, higher compressive strength values are obtained with maximums of 60–70 MPa for CS-12M and CS-15M specimens after 28 and 90 days of curing. Contrariwise, the highest values compressive strength obtained for EAFS binders are close to 40 MPa. Due to the saturation of alkalis, induced by the high concentration of these, all values decreased with high molar concentration (12–15 M for EAFS alkali-activated cements and 15 M for CS alkali-activated cements) (Singh and Singh, 2019). At 28 and 90 days of curing age, a large increase was obtained to samples with higher CaO/FeO molar ratio respect to earlier strengths, showing the importance of Ca in the development of resistance at late ages (Siakati et al., 2021). In the case of EAFS, the highest value was obtained by EAFS-8M at 90 days of curing (41 MPa), closely followed by EAFS-5M (39.5 MPa) specimens. All specimens using EAFS increased considerably their strength due to the fact that they are mainly constituted by CaO and SiO_2, as Portland cement (Wang et al., 2021). The compressive strength decreased as KOH molar concentration increased (12–15 M). When low molar concentration is used, an increase lineal is observed.

By other hand, the highest value obtained by alkali activated cements that used CS as raw material was 75.6 MPa at 90 days of curing for CS-12M specimens. Using as activator KOH 15 M, a high value is also obtained at 90 days (70.2 MPa) and 28 days of curing (69.9 MPa). This could meaning that compressive strength stabilizes at this age when a concentration of 15 M is used. Besides, after one day of curing, great compressive strength values were observed in CS-12M and CS-15M, unlike in CS-5M and CS-8M, where the greatest change occurred between 1 and 7 days of curing. After 7 days of curing, the growth trend was lower in these last two samples. Conversely, a jump was observed between 7 and 28 days of curing for alkali activated materials activated with KOH 12 M and 15 M. The compressive strength is higher in specimens based on CS due to amorphous nature of material that it helps in the dissolution of silicates promoting the geopolymerization reaction and improving the mechanical strength (Singh and Singh, 2019, 2020b). Using CS slag as precursor performed the highest strength because it has a higher amount of silica and lower (FeO + CaO)/SiO_2 molar ratio (Van De Sande et al., 2020). Besides if it is compared these results with other works using Fe-rich slags, high strength has been obtained. CS used in other works content more Ca, for this reason, this suggest that Ca is an important component in the final alkali activated cement

Table 3
Bulk density, apparent porosity and water absorption of alkali activated materials with different molar ratio in the activator: EAFS (a) and CS (b).

A)	CURING AGE	EAFS-5M	EAFS-8M	EAFS-12M	EAFS-15M
Bulk density	1d	1719 ± 17.76	1740 ± 22.70	1701 ± 14.01	1703 ± 5.41
	7d	1785 ± 17.85	1837 ± 24.02	1734 ± 11.66	1743 ± 5.13
	28d	1828 ± 9.06	1885 ± 25.32	1782 ± 15.51	1769 ± 14.74
	90d	1865 ± 15.46	1915 ± 19.28	1855 ± 51.15	1784 ± 13.91
Apparent porosity	1d	39.49 ± 0.52	41.15 ± 0.48	39.28 ± 0.77	34.84 ± 0.23
	7d	34.75 ± 0.79	39.98 ± 0.39	37.82 ± 2.08	33.61 ± 0.13
	28d	33.07 ± 0.35	36.75 ± 0.66	33.75 ± 0.77	33.00 ± 0.36
	90d	32.27 ± 0.68	27.80 ± 0.56	31.18 ± 0.50	32.92 ± 1.01
Absorption	1d	22.93 ± 0.41	24.15 ± 0.45	22.59 ± 0.67	20.66 ± 0.18
	7d	18.89 ± 0.57	23.01 ± 0.36	21.16 ± 1.30	19.25 ± 0.10
	28d	17.51 ± 0.22	18.67 ± 0.85	18.43 ± 0.68	18.41 ± 0.04
	90d	16.82 ± 0.47	14.80 ± 0.34	16.68 ± 0.42	16.66 ± 0.71
B)	CURING AGE	CS-5M	CS-8M	CS-12M	CS-15M
Bulk density	1d	2671 ± 11	2677 ± 15	2742 ± 9	2716 ± 16
	7d	2675 ± 26	2682 ± 4	2743 ± 7	2723 ± 11
	28d	2697 ± 11	2708 ± 36	2744 ± 9	2728 ± 10
	90d	2701 ± 28	2714 ± 12	2750 ± 17	2740 ± 13
Apparent porosity	1d	20.85 ± 0.28	21.71 ± 0.65	18.75 ± 0.50	19.76 ± 0.32
	7d	20.35 ± 0.69	20.25 ± 0.19	18.15 ± 0.32	19.18 ± 0.15
	28d	20.14 ± 0.58	18.73 ± 0.82	17.89 ± 0.22	18.77 ± 0.41
	90d	19.39 ± 0.97	18.40 ± 0.12	17.46 ± 0.35	18.02 ± 0.79
Absorption	1d	7.77 ± 0.14	8.11 ± 0.29	6.86 ± 0.19	6.98 ± 0.15
	7d	7.58 ± 0.32	7.56 ± 0.08	6.67 ± 0.13	6.83 ± 0.08
	28d	7.41 ± 0.24	6.93 ± 0.41	6.56 ± 0.10	6.54 ± 0.17
	90d	7.15 ± 0.41	6.80 ± 0.01	6.36 ± 0.13	7.18 ± 0.31

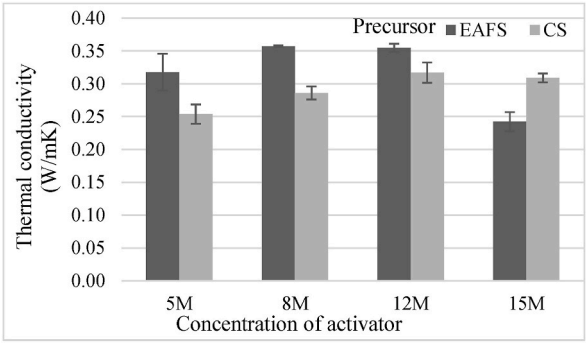

Fig. 7. Thermal conductivity for alkali activated cements based on EAFS and CS at 28 days of curing.

structure (Siakati et al., 2020). The presence of higher amount of silica (27.65 wt%) and Fe (62.18 wt%) in CS is beneficial for the development of the mechanical strength of alkali activated materials, due to its easy dissolution, such as calcium (Adesanya et al., 2020).

In terms of flexural strength, alkali activated cements manufacture with CS are the most resistant, reaching values of 9.5 MPa. The highest value obtained by specimens from EAFS was 8.9 MPa. Both values were observed using different activator KOH 12 M and 8 M, respectively. All results of flexural strength is shown in Fig. 6.

Alkali activated cements from EAFS had a great increase between 28 days and 90 days of curing when KOH 8 M and 12 M were used. Instead using 15 M, the significant increase occurred between 7 days and 28 days. The increase occurs earlier when, the highest concentration is used. Alkali-activated cements are sensitive to the appearance of microcrashes (Gopalakrishnan and Nithiyanantham, 2020), therefore it decreases significantly when the molar concentration in the activator is increased, since microcrashes appear with this increase, as it revealed by SEM images (Figs. 10 and 11). In the case of CS alkali activated cements based, the differences at 90 days are not very large, although microcrash appear but these are very small, difficult to detect.

3.2. Physical properties

The bulk density, apparent porosity and water absorption of alkali-activated cements with different molar ratio of KOH in the activator are shown in Table 3. The trend in bulk density is consistent with the trend observed for the mechanical properties, obtaining highest values EAFS-8M and CS-12M at 90 days of curing. Increasing the curing time for both materials increase the extended structure of the alkali activated cements and reduces the porosity due to good cohesion and adhesion between the different components in the

Table 4
Carbonates content and mass dissolved in HCl of precursors and pastes.

Sample	Carbonate content (wt%)	Mass dissolved in HCl (wt%)	Percentage difference (%)
BS	27.50	99.00	71.50
CS	7.92	89.50	81.58
EAFS-5M	12.23	100.00	87.77
EAFS-8M	10.27	100.00	89.73
EAFS-12M	10.39	100.00	89.61
EAFS-15M	11.91	99.50	87.59
CS-5M	2.38	77.50	75.12
CS-8M	2.68	91.00	88.32
CS-12M	3.06	93.00	89.94
CS-15M	2.60	91.5	88.90

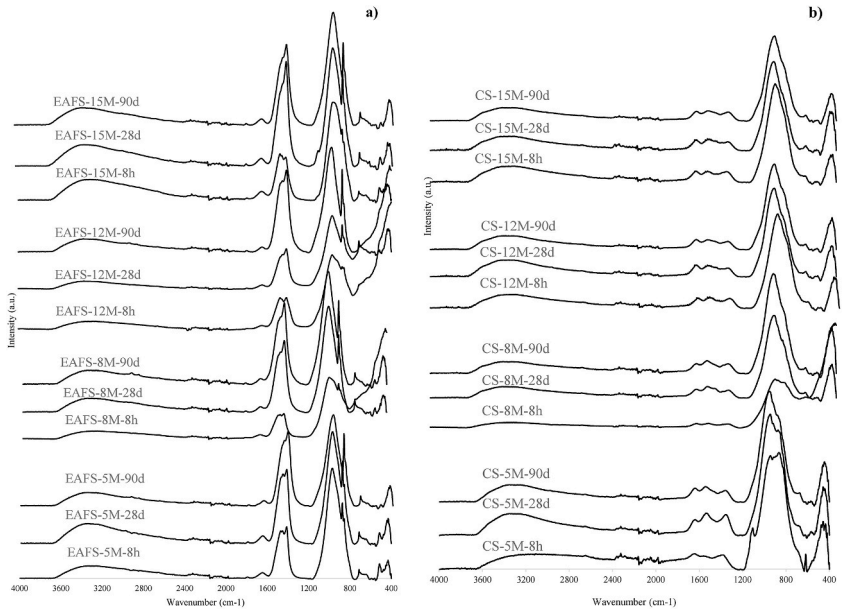

Fig. 8. FTIR spectra of EAFS samples (a) and CS samples (b) at 8 h, 28 days and 90 days.

matrix leading to densification (Gopalakrishnan and Nithiyanantham, 2020). It was also found that the highest bulk density value match with the highest mechanical strength sample, CS-12M. Apparent porosity decreases with increasing alkali content, since this accelerates the reaction and it produces gels that improve the structure (Singh and Singh, 2020b). In addition, the low porosity was attributed to the increase in mechanical resistance.

The real density of EAFS and CS raw materials are 3245 kg/m^3 and 3832 kg/m^3, respectively. There is a lot of difference in physical properties values between EAFS and CS alkali cements. The highest apparent porosity, lowest porosity and lowest absorption may be due to the lower amount of water added to specimens based on CS (l/b ratio of 0.35) (Table 2). This ratio was stablished to achieve adequate workability of pastes, giving rise to denser and more resistant structures.

Thermal conductivity results are shown in Fig. 7. There several factors that affect thermal conductivity values. In this study only alkali concentration was modified, one of parameters that most affects. All specimens presented low thermal conductivity values, if it is compared with others studies (Balcikanli and Ozbay, 2016), and far from the values of traditional Portland cement (G ó mez-Casero et al., 2021). Alkali activated cements manufactured follow the trend of other physical properties, so for example, the higher the bulk density, the higher the thermal conductivity was measured. In addition to this, it was found that the higher the concentration in the activator, the higher the thermal conductivity.

Degree of reaction of the specimens is shown in Table 4. Due to the presence of carbonates in all pastes (see FTIR, Fig. 8), the carbonate content was obtained, because these compounds complicate the response to HCl extraction (Puligilla and Mondal, 2015). The higher the carbonate content in the precursors, greater dissolution in HCl was observed.

In EAFS pastes, a decrease in carbonate content is observed as activator concentration increases. Although, the dissolution in HCl is total in all samples. The CS pastes also presented lower carbonate content and lower dissolution in HCl, due to the lower amount of aluminum in the residue, resulting in a higher amount of Fe-(A)-H-S gel. All alkali-activated cements dissolve more than in the precursors, which could indicate the formation of geopolymeric gel in all specimens (Eliche-Quesada et al., 2021).

Precursors produce pastes with similar carbonate contents, for this reason the content of geopolymeric gel formed can be compared.

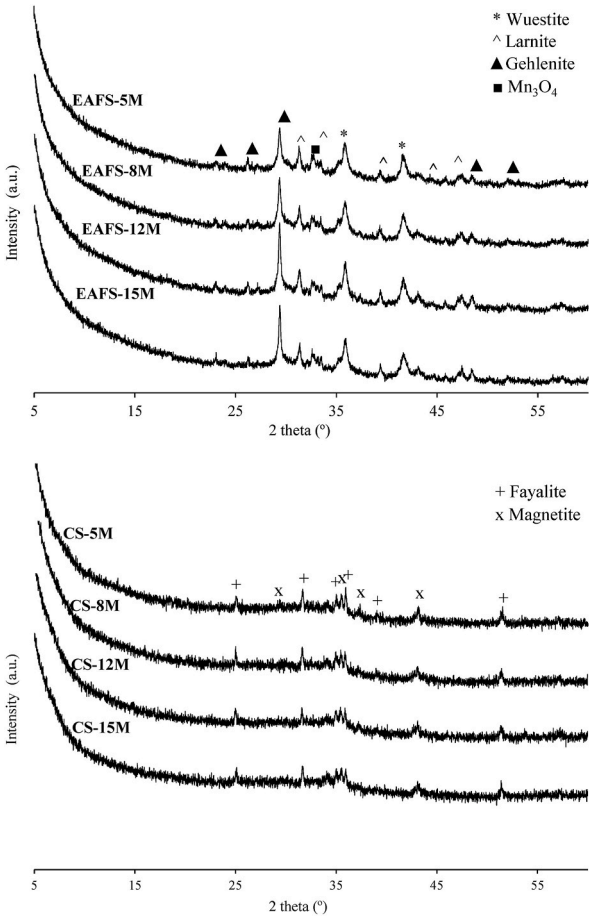

Fig. 9. XRD spectrum of pastes at 28 days.

In EAFS pastes, the specimen with the highest gel content is activated with 8 M; while CS pastes, the highest gel content was obtained with 12 M. These data are in agreement with the results of mechanical strength and SEM micrographs.

3.3. FTIR spectra of samples

FTIR spectra are shown in Fig. 8a and 8b. In all samples were observed two bands centred at 3350 and 1640 cm^{-1}, they are related with H–O–H and O–H bond of water molecules (Singh and Singh, 2020a; G ó mez-Casero et al., 2021). These bands not appear in precursors spectra due to they are reaction products from crystallisation and absorption (Lee and Van Deventer, 2003).

In EAFS samples can be observed that there is a double peak in 1442 and 1398 cm^{-1} at 8 h of curing. The peak in 1442 cm^{-1} disappear when time of curing increase and the halo of 1398 grow. This trend occurred in all specimens observed. The 1442 cm^{-1} band is associated to asymmetric stretching mode of C–O bond of carbonates ($CaCO_3$) present in the matrix unreacted at early curing time. Jamil et al. (2020) related it with presence of calcite due to reaction between extra CaO and atmospheric CO_2. Thus, as the curing age increases, the 1442 cm^{-1} band tends to lose intensity as less and less unreacted carbonate remains. The band centred a 975 cm^{-1} in the precursor (Fig. 4) is moved at lower wavenumbers (970 and 945 cm^{-1}). This band is related to asymmetric stretching mode of Si–O–Si and Si–O–Al bonds (Zheng et al., 2021; Bonet-Mart í nez et al., 2020; Vieira-Ramos et al., 2020). This band identifies the formation of the geopolymeric gel, as well as the incorporation of aluminium (10.7 wt%) in the geopolymeric structure (Dehghani et al., 2021). By other hand, in all EAFS specimens appear a band in 875 cm^{-1}. This band correspond to unreacted slag and it is related with asymmetric stretching of AlO_4 groups (Ismail et al., 2014). This band do not decrease with curing time or concentration of alkaline activator, which suggests that slags react immediately at first stages of curing. The band in 670 cm^{-1} is attributed to C–H bond, characteristic of C–S–H phases (Lin et al., 2020).

In CS binders, a double band centred at 1540 and 1360 cm^{-1} were detected. It is seen less clearly at early ages and low molar concentration in the activator. The 1360 cm^{-1} band shifts to lower wavenumber as curing age increase and alkali content increase, and they are attributed to carbonation process, O–C–O bonds deformation (Nazer et al., 2016). At 950 cm^{-1} an increase in the intensity of band was observed as the curing time increase and molar concentration of KOH increase. This band is identified as new Si–O–Si bonds formation due to the geopolymerization reaction process (Nazer et al., 2016). A band centred at 860 cm^{-1} was identified in lower concentration samples and early ages, which disappears with curing time and higher molar ratio. At 675 cm^{-1} a band was found, but it

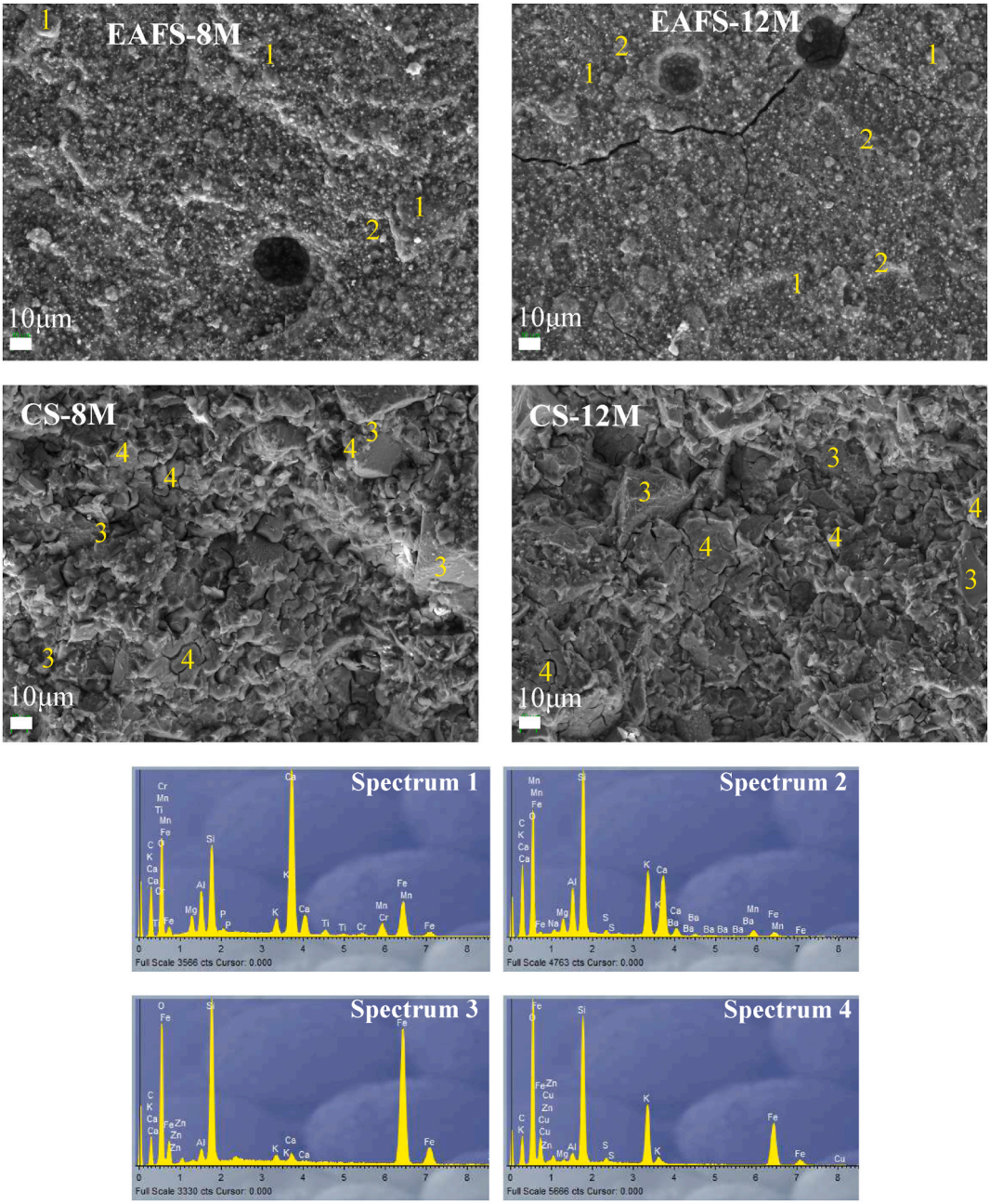

Fig. 10. SEM-EDS of pastes at 28 days.

was not detected at early ages and low concentration of KOH, but as the curing time increases, this peak grows intensity being observed in all specimens. This observation is clearer in samples with higher molar concentration. This peak is attributed to symmetric vibrations of Si–O bonds and it is related with reaction products in the alkaline activation (Singh and Singh, 2020b).

3.4. XRD analysis

XRD spectrums of pastes at 28 days are shown in Fig. 9. Main peaks in precursors (Fig. 2) are also present in pastes, although the intensity of diffraction peaks are lower than raw materials. In pastes manufacture with EAFS, main peaks present are gehlenite and larnite, with any peaks of wuestite. Wuestite peaks are lower than EAFS before alkali reaction and some larnite peaks disappear, due to larnite can dissociate and participate in the formation of C-A-S-H and K-A-S-H gel (Shao et al., 2018).

In the case of CS, spectrum are very similar to raw material showing peaks of fayalite and magnetite, new crystalline peaks were not identified after activation. Although an increase of intensity magnetite peak was observed, due to the oxidation of Fe (Singh and Singh,

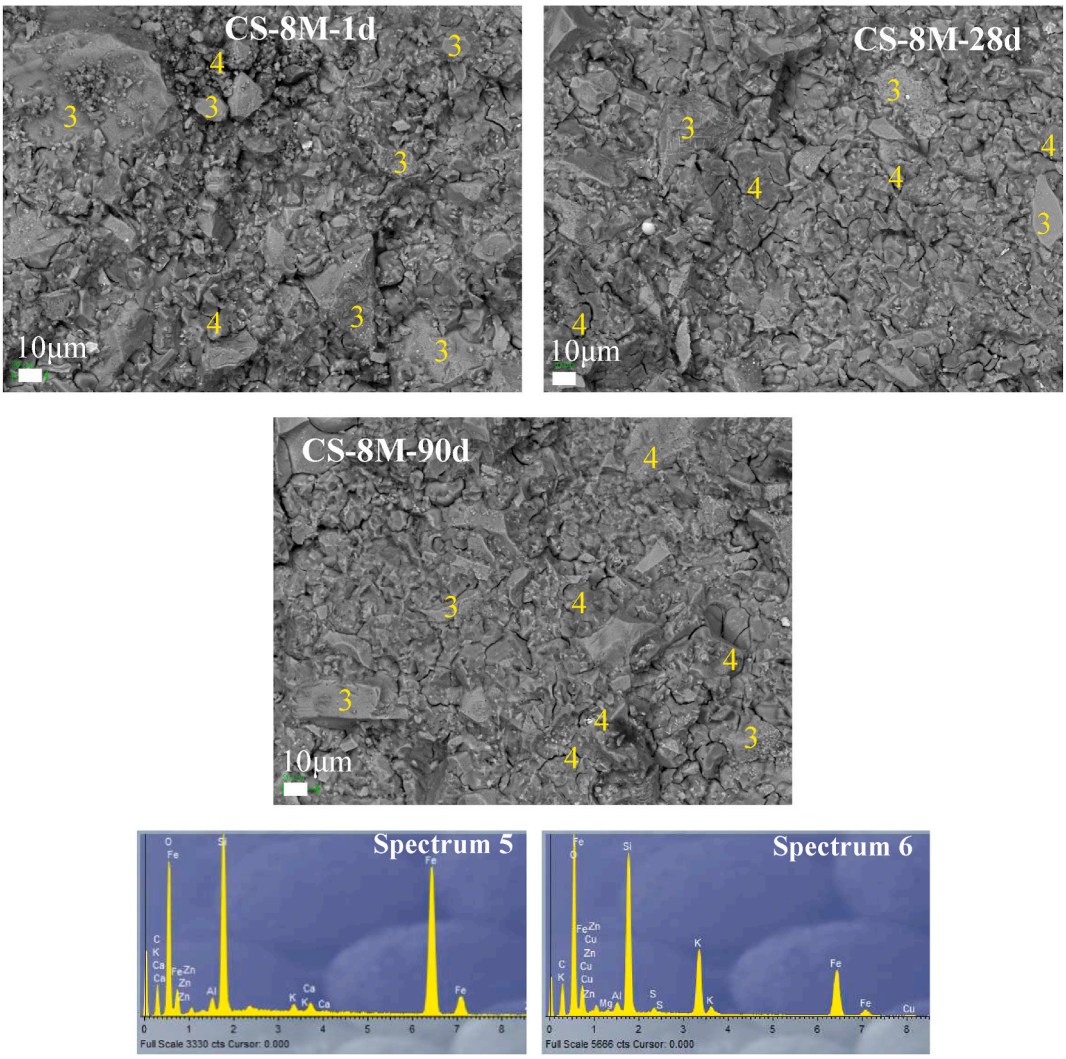

Fig. 11. Electron microscopy images obtained in retrodispersed electron mode from SEM-EDS of CS-8M pastes at 1, 7 and 28 days of curing.

2020a).

3.5. SEM analysis

SEM images of slags activated at 28 days with 8 M and 12 M KOH in the activator are showed in Fig. 10. Great differences can be observed between precursor source. Pastes EAFS-12M present microcrash as a consequence of high molar concentration (Gopalakrishnan and Nithiyanantham, 2020), as was discussed previously at 3.1 section. AAC based on EAFS waste have porous in the matrix, the presence of porous increase increasing the molar concentration of KOH. In general, the matrix is homogeneous. On the other hand, alkali activated cements based on CS have hardly any pores because it has a denser structure, according to bulk density data. Besides, with less molar concentration used, more unreacted particles were found, obtaining a lower strength structure (Sithole and Mashifana, 2020a).

EDS spectra showed two gels in pastes manufacture with EAFS: K-(A)-S-H and C-(A)-S-H. Si, Al and Ca peaks are found in spectrum 1, showing the appearance of C-A-S-H gel. Conversely, K-A-S-H gel is found when in the spectrum 2 peaks of Si, Al and K are showed. In the case of CS, Fe-(A)-S-H gel (spectrum 3) and K,Fe-(A)-S-H gel are detected into the matrix.

Focusing in the best composition, CS-12M, the evolution of alkaline activated material matrix it is appreciated (Fig. 11). At 1 day of curing, there are a significant number of unreacted particles and less dense matrix, as confirming bulk density results. As the curing time increases, the Fe-(A)-S-H gel (spectrum 3) and geopolymeric gel K,Fe-(A)-Si-H are formed. At 28 days of curing appear microcrash in specimens. These microcrash disappear in the alkali activated cements after 90 days of curing, perhaps due to the formation of geopolymeric gel and Fe-(A)-S-H gel that fill the spaces and pores. In fact, crystal whiskers are formed, joining the particles composed by Fe and filling the gaps in the matrix (Zheng et al., 2021).

4. Conclusions

A comparative study using electric arc furnace slags and cupper slags as precursor of alkali-activated cements was performed. The technological properties of alkaline activated cements have been studied as a function of slag type, KOH activator concentration and curing time. The results indicate that different optimal activator was found for each precursor. Optimal properties were obtained for EAFS cements using a molar concentration of 8 M KOH, while a higher concentration of 12 M is necessary to activate CS.

The highest mechanical properties were obtained using CS as precursor (compressive strength:47–70 MPa after 28 days of curing). This could be due to a higher densification of the alkali-activated cements due to a lower amount of water needed to achieve adequate plasticity, to a higher amount of silica and lower (FeO + CaO)/SiO_2 molar ratio, as well as to the formation of Fe-(A)-S-H and geopolymeric Fe,K-(A)-S-H gel. In EAFS C-A-S-H and K-A-S-H gels were formed. The lower compressive strength of the specimens (33–37 MPa after 28 days of curing) could be related to the lower bulk density and fracture microcracks generated both by the shrinkage of the material and water evaporation.

Therefore, this study shows that both waste used as precursors (EAFS and CS) could be used as raw materials for the manufacture of alkali activated cements as alternative material to Portland cement. Valorization of these wastes could reduce greenhouse gases emission and avoid their disposal in landfills. Although better approach could be performed with CS, due to the development of high resistances.

Funding sources

This work was supported by FEDER, Ministry of Science, Innovation and Universities (MAT2017-88097-R, PRE2018-084073 and PID2020-115161RB-I00), State Research Agency, MINECO, CICT of Universidad de JAén (UJA, MINECO, Junta de Andalucía, FEDER). The authors declare that they have no known competing financial interests or personal relationships that could have appeared to influence the work reported in this paper.

Data availability

The datasets generated during and analysed during the current study are available from the corresponding author on reasonable request.

Author contributions

M.A. Gómez-Casero: Conceptualization; methodology; formal analysis and investigation; writing – original draft preparation and writing – review and editing.

L. Pérez-Villarejo: Writing – review and editing; and supervision.

P.J. Sánchez-Soto: Writing – review and editing.

D. Eliche-Quesada: Writing – review and editing; funding acquisition; and supervision.

Declaration of competing interest

The authors declare that they have no known competing financial interests or personal relationships that could have appeared to influence the work reported in this paper.

Acknowledgements

This work has been funded by the project *Development and characterization of new geopolymeric composites based on waste from the olive industry. Towards a sustainable construction* (MAT2017-88097-R), FEDER/Ministry of Science, Innovation and Universities, State Research Agency; and by the project PID2020-115161RB-I00: *Applying the circular economy in the development of new low carbon footprint alkaline activated hydraulic binders for construction solutions (CongActiva)*, MCIN/AEI/10.13039/501100011033 FEDER "A way of making Europe". Authors thank Siderúrgica Sevillana company and Atlantic Copper company for supplying slags. M.A. Gómez-Casero acknowledges support of MINECO (PRE2018-084073). Technical and human support provided by CICT of Universidad de Jaén (UJA, MINECO, Junta de Andalucía, FEDER) is gratefully acknowledged.

References

Abdel-Ghani, N.T., Elsayed, H.A., AbdelMoied, S., 2018. Geopolymer synthesis by the alkali-activation of blastfurnace steel slag and its fire-resistance. Hbrc J. 14 (2), 159–164. https://doi.org/10.1016/j.hbrcj.2016.06.001.

Adesanya, E., Ohenoja, K., Di Maria, A., Kinnunen, P., Illikainen, M., 2020. Alternative alkali-activator from Steel-making Waste for one-part alkali-activated slag. J. Clean. Prod. 274, 123020 https://doi.org/10.1016/j.jclepro.2020.123020.

Amari, S., Darestani, M., Millar, G.J., Rintoul, L., Samali, B., 2019. Microchemistry and microstructure of sustainable mined zeolite-geopolymer. J. Clean. Prod. 234, 1165–1177. https://doi.org/10.1016/j.jclepro.2019.06.237.

Ameri, F., Shoaei, P., Zahedi, M., Karimzadeh, M., Musaeei, H.R., Cheah, C.B., 2021. Physico-mechanical properties and micromorphology of AAS mortars containing copper slag as fine aggregate at elevated temperature. J. Build. Eng. 39, 102289 https://doi.org/10.1016/j.jobe.2021.102289.

Aredes, F.G.M., Campos, T.M.B., Machado, J.P.B., Sakane, K.K., Thim, G.P., Brunelli, D.D., 2015. Effect of cure temperature on the formation of metakaolinite-based geopolymer. Ceram. Int. 41 (6), 7302–7311. https://doi.org/10.1016/j.ceramint.2015.02.022.

Asim, N., Alghoul, M., Mohammad, M., Amin, M.H., Akhtaruzzaman, M., Amin, N., Sopian, K., 2019. Emerging sustainable solutions for depollution: geopolymers. Construct. Build. Mater. 199, 540–548. https://doi.org/10.1016/j.conbuildmat.2018.12.043.

Balaguera, C.A.C., Botero, M.A.G., 2020. Characterization of steel slag for the production of chemically bonded phosphate ceramics (CBPC). Construct. Build. Mater. 241, 118138 https://doi.org/10.1016/j.conbuildmat.2020.118138.
Balcikanli, M., Ozbay, E., 2016. Opimum design of alkali activated slag concretes for the low oxygen/chloride ion permeability and thermal conductivity. Compos. B Eng. 91, 243–256. https://doi.org/10.1016/j.compositesb.2016.01.047.
Bonet-Martínez, E., García-Cobo, P., Pérez-Villarejo, L., Castro, E., Eliche-Quesada, D., 2020. Effect of olive-pine bottom ash on properties of geopolymers based on metakaolin. Materials 13 (4), 901. https://doi.org/10.3390/ma13040901.
Dehghani, A., Aslani, F., Panah, N.G., 2021. Effects of initial SiO2/Al2O3 molar ratio and slag on fly ashbased ambient cured geopolymer properties. Construct. Build. Mater. 293, 123527 https://doi.org/10.1016/j.conbuildmat.2021.123527.
Eliche-Quesada, D., Calero-Rodriguez, A., Bonet-Martínez, E., Pérez-Villarejo, L., Sánchez-Soto, P.J., 2021. Geopolymers made from metakaolin sources, partially replaced by Spanish clays and biomass bottom ash. J. Build. Eng., 102761 https://doi.org/10.1016/j.jobe.2021.102761.
Elkhachine, A., Khachani, N., Saadi, M., Diouri, A., 2022. Mineralogy at early age of alkali activated mortar based on binary additions of limestone quarry dust and electric arc furnace slag. Mater. Today Proc. https://doi.org/10.1016/j.matpr.2022.03.459.
Fakhrabadi, A., Ghadakpour, M., Choobbasti, A.J., Kutanaei, S.S., 2021. Influence of the Non-Woven Geotextile (NWG) on the engineering properties of clayey-sand treated with copper slag-based geopolymer. Construct. Build. Mater. 306, 124830 https://doi.org/10.1016/j.conbuildmat.2021.124830.
Furlani, E., Maschio, S., Magnan, M., Aneggi, E., Andreatta, F., Lekka, M., et al., 2018. Synthesis and characterization of geopolymers containing blends of unprocessed steel slag and metakaolin: the role of slag particle size. Ceram. Int. 44 (5), 5226–5232. https://doi.org/10.1016/j.ceramint.2017.12.131.
Gómez-Casero, M.A., Pérez-Villarejo, L., Castro, E., Eliche-Quesada, D., 2021. Effect of steel slag and curing temperature on the improvement in technological properties of biomass bottom ash based alkali-activated materials. Construct. Build. Mater. 302, 124205 https://doi.org/10.1016/j.conbuildmat.2021.124205.
Gopalakrishnan, R., Nithiyanantham, S., 2020. Microstructural, mechanical, and electrical properties of copper slag admixtured cement mortar. J. Build. Eng. 31, 101375 https://doi.org/10.1016/j.jobe.2020.101375.
Guo, X., Yang, J., 2020. Intrinsic properties and micro-crack characteristics of ultra-high toughness fly ash/steel slag based geopolymer. Construct. Build. Mater. 230, 116965.
Hajimohammadi, A., Ngo, T., Mendis, P., Kashani, A., van Deventer, J.S., 2017. Alkali activated slag foams: the effect of the alkali reaction on foam characteristics. J. Clean. Prod. 147, 330–339. https://doi.org/10.1016/j.jclepro.2017.01.134.
Ismail, I., Bernal, S.A., Provis, J.L., San Nicolas, R., Hamdan, S., van Deventer, J.S.J., 2014. Modification of phase evolution in alkali-activated blast furnace slag by the incorporation of fly ash. Cement Concr. Compos. 45, 125–135. https://doi.org/10.1016/j.cemconcomp.2013.09.006.
ISO 8302. Thermal Insulation Determination of Steady-State Thermal Resistance and Related Properties Guarded Hot Plate Apparatus.
Jamil, N.H., Abdullah, M.M.B., Pa, F.C., Mohamad, H., Ibrahim, W.M.A.W., Chaiprapa, J., 2020. Influences of SiO2, Al2O3, CaO and MgO in phase transformation of sinteres kaolin-ground granulated blast furnace slag geopolymer. J. Mater. Res. Technol. 9, 14922–14932. https://doi.org/10.1016/j.jmrt.2020.10.045.
Khan, M.S.H., Castel, A., Akbarnezhad, A., Foster, S.J., Smith, M., 2016. Utilisation of steel furnace slag coarse aggregate in a low calcium fly ash geopolymer concrete. Cement Concr. Res. 89, 220–229. https://doi.org/10.1016/j.cemconres.2016.09.001.
Khan, K.A., Raut, A., Chandrudu, C.R., Sashidhar, C., 2021. Design and development of sustainable geopolymer using industrial copper byproduct. J. Clean. Prod. 278, 123565 https://doi.org/10.1016/j.jenvman.2015.11.024.
Lancellotti, I., Piccolo, F., Traven, K., Češnovar, M., Ducman, V., Leonelli, C., 2021. Alkali activation of metallurgical slags: reactivity, chemical behavior, and environmental assessment. Materials 14 (3), 639. https://doi.org/10.3390/ma14030639.
Lang, L., Chen, B., Chen, B., 2021. Strength evolutions of varying water content-dredged sludge stabilized with alkali-activated ground granulated blast-furnace slag. Construct. Build. Mater. 275, 122111 https://doi.org/10.1016/j.conbuildmat.2020.122111.
Lee, W.K.W., Van Deventer, J.S.J., 2003. Use of infrared spectroscopy to study geopolymerization of heterogeneous amorphous aluminosilicates. Langmuir 19 (21), 8726–8734.
Li, M., Luo, R., Qin, L., Liu, H., Duan, P., Jing, W., et al., 2021. High temperature properties of graphene oxide modified metakaolin based geopolymer paste. Cem. Concr. Compos., 104318 https://doi.org/10.1016/j.cemconcomp.2021.104318.
Lin, W.Y., Prabhakar, A.K., Mohan, B.C., Wang, C.H., 2020. A factorial experimental analysis of using wood fly ash as an alkaline activator along with coal fly ash for production of geopolymer cementitious hybrids. Sci. Total Environ. 718, 135289 https://doi.org/10.1016/j.scitotenv.2019.135289.
Luukkonen, T., Abdollahnejad, Z., Yliniemi, J., Kinnunen, P., Illikainen, M., 2018. One-part alkali-activated materials: a review. Cement Concr. Res. 103, 21–34. https://doi.org/10.1016/j.cemconres.2017.10.001.
Martins, A.C.P., de Carvalho, J.M.F., Costa, L.C.B., Andrade, H.D., de Melo, T.V., Ribeiro, J.C.L., et al., 2021. Steel slags in cement-based composites: an ultimate review on characterization, applications and performance. Construct. Build. Mater. 291, 123265 https://doi.org/10.1016/j.conbuildmat.2021.123265.
Mozgawa, W., Deja, J., 2009. Spectroscopic studies of alkaline activated slag geopolymers. J. Mol. Struct. 924, 434–441. https://doi.org/10.1016/j.molstruc.2008.12.026.
Nazer, A., Payá, J., Borrachero, M.V., Monzó, J., 2016. Use of ancient copper slags in Portland cement and alkali activated cement matrices. J. Environ. Manag. 167, 115–123. https://doi.org/10.1016/j.jenvman.2015.11.024.
Nedunuri, A.S.S.S., Muhammad, S., 2021. Fundamental understanding of the setting behaviour of the alkali activated binders based on ground granulated blast furnace slag and fly ash. Construct. Build. Mater. 291, 123243 https://doi.org/10.1016/j.conbuildmat.2021.123243.
Nikolić, I., Đurović, D., Marković, S., Veselinović, L., Janković-Častvan, I., Radmilović, V.V., Radmilović, V.R., 2020. Alkali activated slag cement doped with Zn-rich electric arc furnace dust. J. Mater. Res. Technol. 9 (6), 12783–12794. https://doi.org/10.1016/j.jmrt.2020.09.024.
Nikolov, A., Rostovsky, I., Nugteren, H., 2017. Geopolymer materials based on natural zeolite. Case Stud. Constr. Mater. 6, 198–205. https://doi.org/10.1016/j.cscm.2017.03.001.
Oyebisi, S., Ede, A., Olutoge, F., Ogbiye, S., 2020. Evaluation of reactivity indexes and durability properties of slag-based geopolymer concrete incorporating corn cob ash. Construct. Build. Mater. 258, 119604 https://doi.org/10.1016/j.conbuildmat.2020.119604.
Pacheco-Torgal, F., Abdollahnejad, Z., Camões, A.F., Jamshidi, M., Ding, Y., 2012. Durability of alkali-activated binders: a clear advantage over Portland cement or an unproven issue? Construct. Build. Mater. 30, 400–405. https://doi.org/10.1016/j.conbuildmat.2011.12.017.
Phiri, T.C., Singh, P., Nikoloski, A.N., 2021. The potential for copper slag waste as a resource for a circular economy: a review–Part II. Miner. Eng. 172, 107150 https://doi.org/10.1016/j.mineng.2021.107150.
Provis, J.L., 2018. Alkali-activated materials. Cement Concr. Res. 114, 40–48. https://doi.org/10.1016/j.cemconres.2017.02.009.
Puertas, F., 1995. Cementos de escorias activadas alcalinamente: Situación actual y perspectivas de futuro.
Puertas, F., González-Fonteboa, B., González-Taboada, I., Alonso, M.M., Torres-Carrasco, M., Rojo, G., Martínez-Abella, F., 2018. Alkali-activated slag concrete: fresh and hardened behaviour. Cem. Concr. Compos. 85, 22–31. https://doi.org/10.1016/j.cemconcomp.2017.10.003.
Puligilla, S., Mondal, P., 2015. Co-existence of aluminosilicate and calcium silicate gel characterized through selective dissolution and FTIR spectral subtraction. Cement Concr. Res. 70, 39–49. https://doi.org/10.1016/j.cemconres.2015.01.006.
Rees, C.A., 2007. Mechanisms and Kinetics of Gel Formation in Geopolymers (Doctoral Dissertation).
Salman, M., Cizer, Ö., Pontikes, Y., Vandewalle, L., Blanpain, B., Van Balen, K., 2014. Effect of curing temperatures on the alkali activation of crystalline continuous casting stainless steel slag. Construct. Build. Mater. 71, 308–316. https://doi.org/10.1016/j.conbuildmat.2014.08.067.
Salman, M., Cizer, Ö., Pontikes, Y., Snellings, R., Vandewalle, L., Blanpain, B., Van Balen, K., 2015. Cementitious binders from activated stainless steel refining slag and the effect of alkali solutions. J. Hazard Mater. 286, 211–219. https://doi.org/10.1016/j.jhazmat.2014.12.046.
Seo, J., Bae, S.J., Jang, D.I., Park, S., Yang, B., Lee, H.K., 2020. Thermal behavior of alkali-activated fly ash/slag with the addition of an aerogel as an aggregate replacement. Cem. Concr. Compos. 106, 103462 https://doi.org/10.1016/j.cemconcomp.2019.103462.
Shao, N., Tang, S., Liu, Z., Li, L., Yan, F., Liu, F., et al., 2018. Hierarchically structured calcium silicate hydrate-based nanocomposites derived from steel slag for highly efficient heavy metal removal from wastewater. ACS Sustain. Chem. Eng. 6 (11), 14926–14935. https://doi.org/10.1021/acssuschemeng.8b03428.

Siakati, C., Douvalis, A.P., Ziogas, P., Peys, A., Pontikes, Y., 2020. Impact of the solidification path of FeOx–SiO2 slags on the resultant inorganic polymers. J. Am. Ceram. Soc. 103 (3), 2173–2184. https://doi.org/10.1111/jace.16869.

Siakati, C., Douvalis, A.P., Hallet, V., Peys, A., Pontikes, Y., 2021. Influence of CaO/FeO ratio on the formation mechanism and properties of alkali-activated Fe-rich slags. Cement Concr. Res. 146, 106466 https://doi.org/10.1016/j.cemconres.2021.106466.

Singh, J., Singh, S.P., 2019. Development of alkali-activated cementitious material using copper slag. Construct. Build. Mater. 211, 73–79. https://doi.org/10.1016/j.conbuildmat.2019.03.233.

Singh, J., Singh, S.P., 2020a. Synthesis of alkali-activated binder at ambient temperature using copper slag as precursor. Mater. Lett. 262, 127169 https://doi.org/10.1016/j.matlet.2019.127169.

Singh, J., Singh, S.P., 2020b. Evaluating the alkali-silica reaction in alkali-activated copper slag mortars. Construct. Build. Mater. 253, 119189 https://doi.org/10.1016/j.conbuildmat.2020.119189.

Sithole, N.T., Mashifana, T., 2020a. Geosynthesis of building and construction materials through alkaline activation of granulated blast furnace slag. Construct. Build. Mater. 264, 120712 https://doi.org/10.1016/j.conbuildmat.2020.120712.

Sithole, N.T., Mashifana, T., 2020b. Geosynthesis of building and construction materials through alkaline activation of granulated blast furnace slag. Construct. Build. Mater. 264, 120712 https://doi.org/10.1016/j.conbuildmat.2020.120712.

Szabó, L., Hidalgo, I., Ciscar, J.C., Soria, A., 2006. CO2 emission trading within the European Union and Annex B countries: the cement industry case. Energy Pol. 34 (1), 72–87. https://doi.org/10.1016/j.enpol.2004.06.003.

UNE-EN 1015-11:2000A1:2007 Methods of Test for Mortar for Masonry - Part 11: Determination of Flexural and Compressive Strength of Hardened Mortar, 2007. Spanish Association for Normalization and Certification.

UNE-EN 1015-10:1999, 1999. Methods of Test for Mortar for Masonry – Part 10: Determination of Dry Bulk Density of Hardened Mortar.

Van De Sande, J., Peys, A., Hertel, T., Rahier, H., Pontikes, Y., 2020. Upcycling of non-ferrous metallurgy slags: identifying the most reactive slag for inorganic polymer construction materials. Resour. Conserv. Recycl. 154, 104627 https://doi.org/10.1016/j.resconrec.2019.104627.

Vieira-Ramos, F.J.H.T., Marques-Vieira, M.F., Tienne, L.G.P., Aguiar, V.O., 2020. Evaluation and characterization of geopolymer foams synthesized from blast furnace with sodium metasilicate. J. Mater. Res. Technol. 9, 12019–12029. https://doi.org/10.1016/j.jmrt.2020.08.019.

Wang, H.Y., Wang, W.C., Wang, J.C., Chen, Y.W., 2021. Evaluation of the engineering properties and durability of mortar produced using ground granulated blast-furnace slag and stainless steel reduced slag. Construct. Build. Mater. 280, 122498 https://doi.org/10.1016/j.conbuildmat.2021.122498.

Yan, Z., Sun, Z., Yang, J., Yang, H., Ji, Y., Hu, K., 2021. Mechanical performance and reaction mechanism of copper slag activated with sodium silicate or sodium hydroxide. Construct. Build. Mater. 266, 120900 https://doi.org/10.1016/j.conbuildmat.2020.120900.

You, N., Liu, Y., Gu, D., Ozbakkaloglu, T., Pan, J., Zhang, Y., 2020. Rheology, shrinkage and pore structure of alkali-activated slag-fly ash mortar incorporating copper slag as fine aggregate. Construct. Build. Mater. 242, 118029 https://doi.org/10.1016/j.conbuildmat.2020.118029.

Zhang, S., Zhu, N., Mao, F., Zhang, J., Huang, X., Li, F., et al., 2021. A novel strategy for harmlessness and reduction of copper smelting slags by alkali disaggregation of fayalite (Fe2SiO4) coupling with acid leaching. J. Hazard Mater. 402, 123791 https://doi.org/10.1016/j.jhazmat.2020.123791.

Zhang, S., Ghouleh, Z., Mucci, A., Bahn, O., Provençal, R., Shao, Y., 2022. Production of cleaner high-strength cementing material using steel slag under elevated-temperature carbonation. J. Clean. Prod. 342, 130948 https://doi.org/10.1016/j.jclepro.2022.130948.

Zheng, W., He, D., Wang, Y., Chen, J., Xue, M., Li, H., 2021. Preparation of cement-based color facing mortar by copper pyrometallurgical slag modification: efficient utilization of high-ironcontent slag. J. Environ. Chem. Eng., 105888 https://doi.org/10.1016/j.jece.2021.105888.